STRUCTURAL BIOLOGY

Structural insights into the functional versatility of an FHA domain protein in mycobacterial signaling

Tristan Wagner[1]*†, Gwénaëlle André-Leroux[1]*‡, Valérie Hindie[1]§, Nathalie Barilone[1]‖, María-Natalia Lisa[1]¶, Sylviane Hoos[2], Bertrand Raynal[2], Brigitte Vulliez-Le Normand[1], Helen M. O'Hare[3], Marco Bellinzoni[1]#, Pedro M. Alzari[1]#

Forkhead-associated (FHA) domains are modules that bind to phosphothreonine (pThr) residues in signaling cascades. The FHA-containing mycobacterial protein GarA is a central element of a phosphorylation-dependent signaling pathway that redirects metabolic flux in response to amino acid starvation or cell growth requirements. GarA acts as a phosphorylation-dependent ON/OFF molecular switch. In its nonphosphorylated ON state, the GarA FHA domain engages in phosphorylation-independent interactions with various metabolic enzymes that orchestrate nitrogen flow, such as 2-oxoglutarate decarboxylase (KGD). However, phosphorylation at the GarA N-terminal region by the protein kinase PknB or PknG triggers autoinhibition through the intramolecular association of the N-terminal domain with the FHA domain, thus blocking all downstream interactions. To investigate these different FHA binding modes, we solved the crystal structures of the mycobacterial upstream (phosphorylation-dependent) complex PknB-GarA and the downstream (phosphorylation-independent) complex GarA-KGD. Our results show that the phosphorylated activation loop of PknB serves as a docking site to recruit GarA through canonical FHA-pThr interactions. However, the same GarA FHA–binding pocket targets an allosteric site on nonphosphorylated KGD, where a key element of recognition is a phosphomimetic aspartate. Further enzymatic and mutagenesis studies revealed that GarA acted as a dynamic allosteric inhibitor of KGD by preventing crucial motions in KGD that are necessary for catalysis. Our results provide evidence for physiological phosphomimetics, supporting numerous mutagenesis studies using such approaches, and illustrate how evolution can shape a single FHA-binding pocket to specifically interact with multiple phosphorylated and nonphosphorylated protein partners.

INTRODUCTION

Reversible serine-threonine protein phosphorylation mediated by Hanks-type serine-threonine protein kinases (STPKs) and phosphatases has emerged as a major regulatory mechanism in bacteria (*1*–*3*). As shown by extensive studies in eukaryotic cells, phosphorylation at serine, threonine, or tyrosine residues can directly alter the biochemical function of a protein, but more often, it creates new docking sites for phosphorylation-dependent binding partners (*4*). This supports the idea that phosphorylation-based signal transduction systems can be thought of as tripartite toolkits composed of protein kinases acting as "writers," protein phosphatases as "erasers," and phospho-binding domains as downstream "readers" of the posttranslational modification (*5*). Since the discovery of Src homology 2 (SH2) domains (*6*), which specifically bind phosphotyrosine residues, many different types of reader domains have been described in eukaryotic cell signaling. The current list of known modules that specifically bind to phosphoserine (pSer) and phosphothreonine (pThr) residues includes no less than 14 unrelated domain types (*5*). However, in bacteria, the widespread distribution of STPKs contrasts with the finding that only one of those reader protein modules has so far been found, namely, the Forkhead-associated (FHA) domain (*7*).

First identified within the Forkhead family of transcription factors (*8*), FHA domains serve as adaptor modules that specifically recognize pThr-containing proteins and mediate protein-protein interactions that are driven by reversible phosphorylation of many eukaryotic regulatory proteins with roles in the DNA damage response, checkpoint signaling pathways, cell growth, and cell cycle regulation (*9*). FHA modules share a conserved fold consisting of a 10- or 11-stranded β-barrel that contains the pThr-binding pocket at one of the apical surfaces (*10*, *11*). The atomic structures of more than 50 FHA domains are currently available, and most of these were determined either in the absence of a cognate binding partner or by using a phosphopeptide to represent the binding partner. This strategy is apparently justified by structures in which the target pThr recognized by the FHA lies in an unstructured N- or C-terminal region (*12*–*14*). Some FHA domains bind nonphosphorylated protein partners using surfaces distinct from the pThr-binding pocket. This may occur in FHA domains that lack the conserved phosphate-interacting residues, such as that of the kinesin KIF13 (*15*), or that use their canonical pThr-binding site to interact with a third protein partner, such as the FHA1 domain of Rad51 (*16*).

In prokaryotes, FHA domain–containing proteins are ubiquitous in three main phyla, namely, the Actinobacteria, Cyanobacteria, and selected Gram-negative Proteobacteria (*7*), but their precise roles in bacterial physiology are generally not well characterized. We focused

[1]Institut Pasteur, Unité de Microbiologie Structurale, CNRS UMR 3528 & Université Paris Diderot, 25 Rue du Docteur Roux, 75724 Paris Cedex 15, France. [2]Institut Pasteur, Plateforme de Biophysique Moléculaire, 25 Rue du Docteur Roux, 75724 Paris Cedex 15, France. [3]Leicester Tuberculosis Research Group (LTBRG) and Leicester Institute of Structural and Chemical Biology (LISCB), Department of Respiratory Science & Department of Molecular and Cell Biology, University of Leicester, Leicester LE1 7RH, UK.
*These authors contributed equally to this work.
†Present address: Max Planck Institute for Marine Microbiology, Microbial Metabolism Group, Celsiusstrasse 1, D-28359 Bremen, Germany.
‡Present address: INRA, Unité de Mathématique et Informatique Appliquées du Génome à l'Environnement, Université Paris-Saclay, 78350 Jouy-en-Josas Cedex, France.
§Present address: Caprion Biosciences Inc., 201 Ave. President Kennedy, Montreal H2X 3Y7, Canada.
‖Present address: Unité Récepteurs-Canaux, Institut Pasteur, 75724 Paris Cedex 15, France.
¶Present address: Instituto de Biología Molecular y Celular de Rosario (IBR, CONICET-UNR), Ocampo y Esmeralda, S2002LRK Rosario, Argentina.
#Corresponding author. Email: pedro.alzari@pasteur.fr (P.M.A.); marco.bellinzoni@pasteur.fr (M.B.)

on GarA, member of an Actinobacterial-restricted family of FHA domain–containing proteins that play a central role in the kinase-mediated control of glutamate metabolism (*17*, *18*). Mycobacterial GarA was initially described as a glycogen accumulation regulator (hence its name) in *Mycobacterium smegmatis* (*19*) and identified as an optimal substrate of the serine-threonine protein kinase PknB in *Mycobacterium tuberculosis* protein extracts (*20*). Subsequently, it was characterized as a key regulator of glutamate metabolism in *M. tuberculosis*, *M. smegmatis* (*13*, *18*, *21*, *22*), and *Corynebacterium glutamicum*, wherein the GarA ortholog was named OdhI for 2-oxoglutarate dehydrogenase (ODH) inhibitor (*23*, *24*). GarA is essential to sustain *M. tuberculosis* growth and viability, but it is dispensable in *M. smegmatis* and *C. glutamicum*, in which disruption of *garA* or *odhI*, respectively, causes a distinctive, nutrient-dependent phenotype (*23*, *25*).

GarA protein family members are small proteins (~160 amino acids) consisting of a C-terminal FHA domain linked to an unstructured N-terminal extension of 40 to 50 residues that includes a consensus phosphorylation motif ETTSVFR (Fig. 1A and fig. S1). GarA is a key element of a conserved STPK-mediated signaling pathway that controls glutamate metabolism (Fig. 1B). Nonphosphorylated GarA was shown to activate the glutamate synthase (GS) complex (*13*) and to inhibit the activities of E1o, the first component of the ODH multiprotein complex, and glutamate dehydrogenase (GDH), a nicotinamide adenine dinucleotide (NAD)–dependent GDH (*18*) in mycobacteria. Although only the interaction of the GarA homolog OdhI with E1o has been reported in *C. glutamicum* (*23*), the net outcome of the nonphosphorylated OdhI activity is the same as for GarA, namely, a redirection of the metabolic flux toward the synthesis of glutamate (Fig. 1B). In response to nutrient availability or cell growth requirements (*22*), phosphorylation at the first or second Thr residue within the ETTSVFR motif by the STPKs PknG or PknB, respectively (Fig. 1B), triggers the intramolecular association of the N-terminal extension with the C-terminal FHA domain, switching off the modulatory interactions with downstream metabolic enzymes (*12*, *13*, *26*). Therefore, at different stages of the signaling pathway (Fig. 1B), GarA acts as either a specific STPK protein substrate, a phosphorylation-dependent molecular ON/OFF switch, or an allosteric metabolic modulator. Quite unusually, GarA performs all these tasks using its FHA domain to specifically recognize upstream pThr-containing proteins (PknB and PknG) and downstream nonphosphorylated protein partners (GS, E1o, and GDH). To gather structural insights into this functional versatility, we report here structural and biochemical studies of the upstream (phosphorylation-dependent) signaling complex PknB-GarA and the downstream (phosphorylation-independent) effector complex GarA-E1o. These studies revealed that the same binding pocket of the GarA FHA domain mediated both docking to the phosphorylated activation loop of PknB through a canonical FHA-pThr interaction and allosteric inhibition of the nonphosphorylated *M. smegmatis* homolog of E1o through recognition of a phosphomimetic aspartate in the substrate. Together, these observations illustrate how a canonical FHA domain–binding pocket can be fine-tuned to specifically interact with both phosphorylated and nonphosphorylated protein partners, extending the functions of prokaryotic FHA domain proteins beyond a simple role of phosphorylation reader domains, with important implications for bacterial cell signaling.

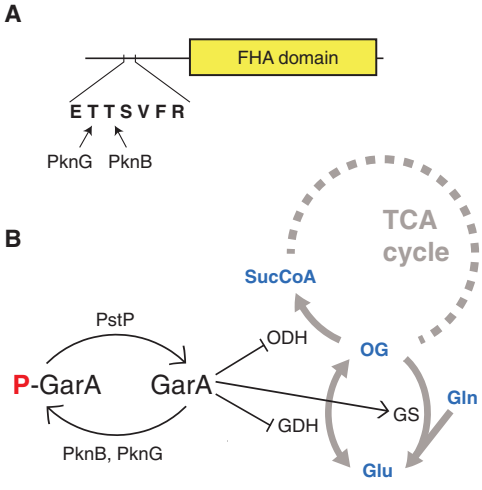

Fig. 1. GarA regulates glutamate metabolism in Actinobacteria. (**A**) GarA consists of a C-terminal FHA domain and an N-terminal peptide extension that contains two adjacent phosphorylatable threonine residues: Thr^{21} and Thr^{22} in *M. tuberculosis* GarA (*18*, *20*) [equivalent to Thr^{14} and Thr^{15} in the *C. glutamicum* homolog OdhI (*17*)]. PknG phosphorylates the first Thr in each protein, whereas PknB targets the second Thr residue in each protein. (**B**) Mycobacterial signaling pathway involving GarA, which functions as a phospho-dependent (ON/OFF) molecular switch (*26*). In the ON state, nonphosphorylated GarA represses or stimulates the activity of three distinct metabolic enzymes and redirects the metabolic flux (thick gray lines) toward the synthesis of glutamate. GarA binding to its downstream targets does not depend on a pThr residue in the target, which is rare among FHA domains. Phosphorylation of GarA by PknG or PknB triggers an intramolecular interaction, resulting in a closed (autoinhibited) conformation that blocks the pThr-binding site of the FHA domain and switches off the regulatory properties of GarA. Dephosphorylation of GarA by PstP, the conserved transmembrane protein serine-threonine phosphatase in Actinobacteria, is assumed based on PstP-mediated dephosphorylation of the GarA homolog OdhI in *C. glutamicum* (*63*). OG, 2-oxoglutarate; Glu, glutamate; Gln, glutamine; SucCoA, succinyl–coenzyme A.

RESULTS

The phospho-dependent signaling complex PknB-GarA

In previous work, we showed that *M. tuberculosis* GarA is an efficient substrate of various STPKs, mainly PknB and PknG (*18*, *20*). Phosphorylation occurs at Thr^{21} (PknG) or Thr^{22} (PknB) in the disordered N-terminal extension of GarA, requiring in both cases specific docking interactions between phosphorylated residues in the kinase and the substrate's FHA domain. The autophosphorylated docking sites in PknG are located outside the catalytic domain (*18*), but those in PknB ($pThr^{171}$ and $pThr^{173}$) are both in the kinase activation loop (*20*), and their interaction with the GarA FHA domain would thus be expected to sequester the activation loop away from the active kinase conformation (*27*). To address this issue, we sought to characterize the structure of *M. tuberculosis* GarA in complex with the catalytic domain (residues 1 to 279) of wild-type PknB (hereafter referred to as $PknB_{CD}$). The autophosphorylated $PknB_{CD}$-GarA interaction was observed in solution (fig. S2) with a dissociation constant (K_D) in the micromolar range (fig. S3). Upon extensive crystallization trials, however, all the crystals we obtained contained $PknB_{CD}$ in a "back-to-back" homodimer conformation (*28*, *29*) with no bound GarA. The reported K_D for dimerization is high (2.9 mM) (*30*), suggesting that dimerization of $PknB_{CD}$ in different crystal forms (*28*–*31*) may result from the high protein concentrations used for crystallization. To explore whether kinase dimerization could exclude GarA binding,

we produced a monomeric form of $PknB_{CD}$ by making a point mutation that replaced Leu^{33} with glutamic acid ($PknB_{CD,L33E}$). The L33E mutation abrogated PknB dimerization (*30*) but retained wild-type–like phosphorylation activity toward GarA (see the next section). This monomeric form of PknB was successfully crystallized in complex with GarA and the non-hydrolyzable adenosine 5′-triphosphate (ATP) analog AMP-PCP, and the crystal structure of the ternary complex was determined at 2.3 Å resolution (table S1).

The crystal structure contained two molecules of the ternary complex in the asymmetric unit and revealed that the FHA domain of GarA interacted primarily with the phosphorylated activation loop of PknB (Fig. 2A). Despite using a non-hydrolyzable ATP analog,

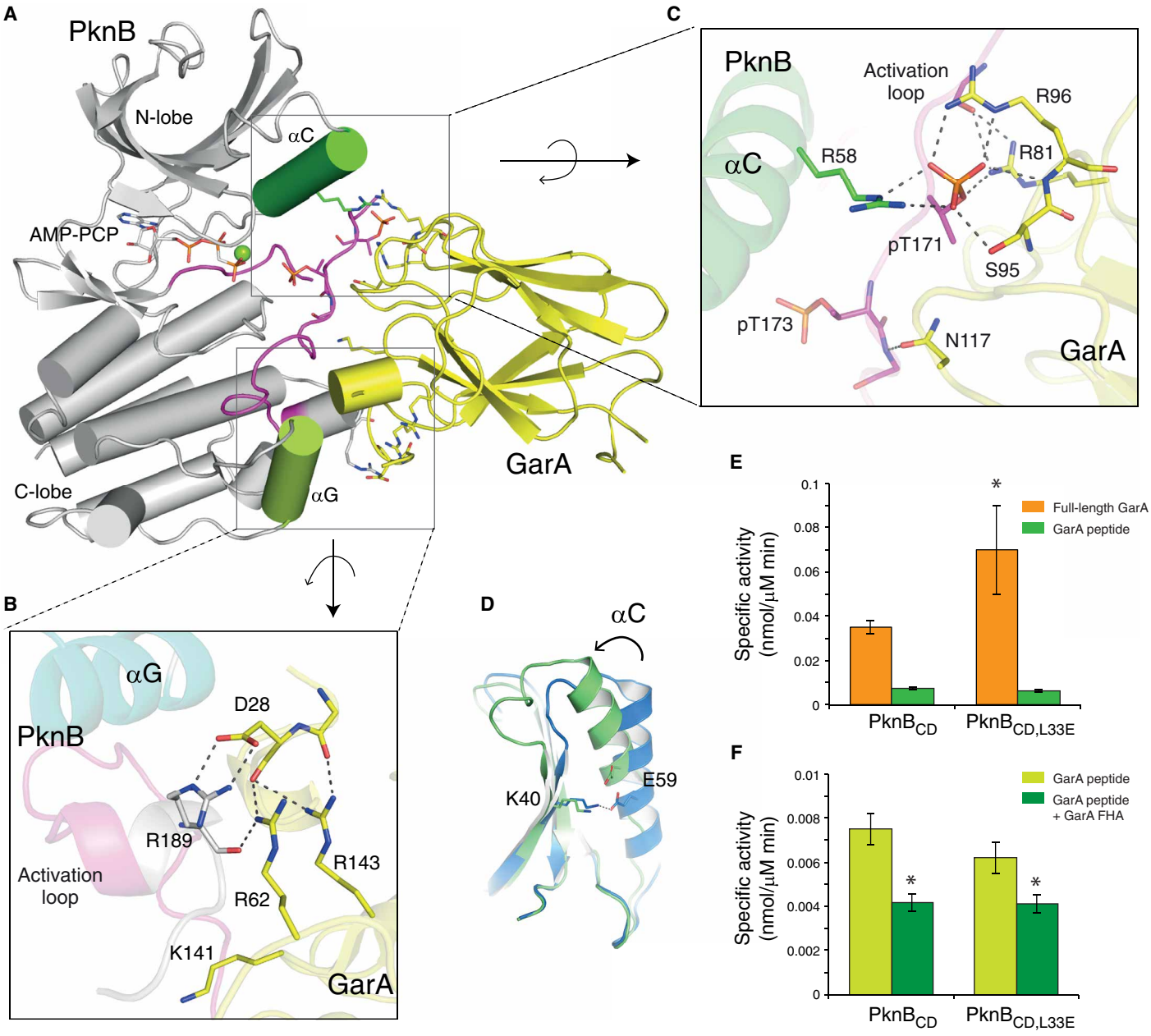

Fig. 2. Structure of the ternary GarA-PknB-nucleotide complex. (**A**) Overall view of the GarA-$PknB_{CD,L33E}$ complex. The complex was crystallized in the presence of the non-hydrolyzable ATP analog AMP-PCP. GarA is shown in yellow, the PknB kinase activation loop is shown in violet, and the two PknB helices involved in the interface are shown in green. The non-hydrolyzable ATP analog and the residues involved in Thr-phosphate binding are depicted as sticks. (**B**) The N-terminal GarA peptide (residues 26 to 34) mediates the interaction between a patch of basic residues on the FHA domain surface (Arg^{62}, Arg^{143}) and the αG helix of PknB. (**C**) Close-up view of the $pThr^{171}$-binding site, showing all phosphate oxygens involved in hydrogen-bonding interactions. (**D**) Structural differences in the PknB helix αC between the PknB-GarA complex (green) and the back-to-back PknB homodimer (blue, PDB code 1O6Y). (**E**) Kinase activity of $PknB_{CD}$ and $PknB_{CD,L33A}$ on full-length GarA (orange) and on the 17-residue N-terminal peptide substrate (green). (**F**) Kinase activity of $PknB_{CD}$ and $PknB_{CD,L33A}$ on the peptide substrate in the absence (light green) and presence (dark green) of the GarA FHA domain. In (E) and (F), values are the mean of three independent measurements ($n = 3$), and error bars represent the SEM. Significance of differences between the mean values (E and F) was analyzed statistically (*$P < 0.05$, Student's t test).

no electron density was visible for the ETTSVFR peptide substrate (GarA residues 20 to 26) in the kinase active site. The entire N-terminal extension of GarA, residues 1 to 45, was mostly disordered in the crystal structure, in agreement with the high flexibility observed for this region in the nuclear magnetic resonance (NMR) structures of nonphosphorylated *M. tuberculosis* GarA and *C. glutamicum* OdhI (*12*, *13*). The only exception was a short peptide fragment (corresponding to GarA residues 26 to 34) that was visible in the electron density map for one of the two independent complexes, between helix αG in PknB and a positively charged region of the FHA domain of GarA (Fig. 2, A and B). This position would be compatible with GarA Thr^{22} reaching the kinase active site, because the same peptide fragment occupies a similar position against the FHA domain core in the NMR structures of phosphorylated GarA and OdhI (fig. S4, A to C).

A canonical phosphate-binding pocket in the FHA domain

The phosphorylated activation loop, which was systematically disordered in other PknB crystal structures (*28*–*31*), exhibited an extended conformation at the PknB-GarA interface (Fig. 2A). The observed conformation, positioning the phosphate groups of $pThr^{171}$ and $pThr^{173}$ far (>10 Å) from the guanidinium group of the HRD (His-Arg-Asp) motif, differentiates PknB from eukaryotic kinases that require interaction between HRD and pThr for activation. The loop followed a path across the surface of the FHA domain that is similar to that previously observed in other FHA domain–phosphopeptide complex structures (fig. S5, A and B). The phosphate-binding site of the FHA domain, mainly defined by the loops between strands β4-β5 and β6-β7 (fig. S6), bound $pThr^{171}$ from the PknB activation loop (Fig. 2C). The phosphate group was stabilized by intermolecular hydrogen-bonding interactions with several GarA residues: the guanidinium groups of Arg^{81} and Arg^{96}, the hydroxyl group of Ser^{95}, and the main-chain nitrogen atom of Arg^{96}. Additional hydrogen bonds were formed between the phosphopeptide backbone adjacent to $pThr^{171}$ in the kinase and the side chains of Arg^{81} and Asn^{117} in the Gar A FHA domain. All these interactions involve residues from three conserved motifs in bacterial FHA domains (*7*), namely, $G^{80}R$ at the C terminus of strand β3, $S^{95}RxH$ just preceding β5, and motif $S^{115}xNG$ in the β6-β7 turn (fig. S1), indicating a canonical mode of pThr recognition.

Uniquely among FHA-pThr complexes, however, an additional structural element directly interacts with the phosphorylated residue. The guanidinium group of Arg^{58} on PknB helix αC made a strong salt bridge with $pThr^{171}$ (Fig. 2C), promoting major structural changes in the helix (see the next section). In addition, the total $PknB_{CD}$-GarA interface of 1100 $Å^2$ (including the N-terminal GarA peptide 26–34) was higher than those typically observed for FHA-phosphopeptide complexes. The additional contacts were primarily mediated by the positively charged region formed by the loops β1-β2 and β9-β10 in the FHA domain of GarA that interact with the C terminus of the PknB activation loop, preceding helix αE, and with helix αG through the N-terminal GarA peptide (Fig. 2B).

Upon binding of the GarA FHA domain, the PknB regulatory helix αC moved away from the conformation observed in the back-to-back PknB homodimer (*28*). The helical axis was displaced 6 Å toward the core of the PknB N-lobe, and the helix underwent partial unwinding at its C terminus (Fig. 2D). As a consequence, the overall conformation of the kinase N-lobe in complex with GarA appears to be incompatible with that observed in the PknB homodimer, possibly accounting for our unsuccessful attempts to crystallize the complex between GarA and wild-type $PknB_{CD}$. Furthermore, these GarA-induced changes in helix αC weaken a well-conserved intramolecular salt bridge in the kinase domain, the integrity of which is usually important for activity because it positions the α- and β-phosphate groups of ATP correctly for catalysis (*32*). This bridge between Lys^{40} and Glu^{59} from helix αC was 4.2 Å in the $PknB_{CD}$-GarA complex, compared to 2.8 Å in homodimeric $PknB_{CD}$. Similar conformational changes have been described for two $PknB_{CD}$ point mutants (*30*), suggesting a high conformational plasticity of the active kinase.

The kinase activation loop as a docking site for FHA-mediated substrate recruitment

To determine the effects of the observed conformational changes on kinase activity, we measured the phosphorylation activity of $PknB_{CD}$ and $PknB_{CD,L33E}$ toward full-length GarA compared to that toward an N-terminal GarA peptide that contained the phosphorylation site but lacked the FHA domain. The activity of the point mutant $PknB_{CD,L33E}$ on each substrate was roughly equivalent to that of wild-type $PknB_{CD}$ on the same substrate (Fig. 2E), confirming that the amino acid substitution L33E had no major effect on the kinase activity under the assayed conditions. In contrast, the two versions of $PknB_{CD}$ were both markedly less active toward the GarA-derived peptide substrate compared to full-length GarA (Fig. 2E), indicating that GarA phosphorylation is strongly dependent on the interaction between the kinase activation loop and the FHA domain. An important question here is whether the phosphorylated activation loop is acting as a passive docking platform for substrate recruitment (with no increase of the intrinsic kinase activity) or, alternatively, whether FHA domain binding has an allosteric effect on the kinase activity. To elucidate this issue, we produced a GarA deletion mutant that comprises only the FHA domain but is devoid of the N-terminal phosphorylatable extension, and assayed the kinase activity of $PknB_{CD}$ and $PknB_{CD,L33E}$ on the peptide substrate in the presence or absence of the FHA-only mutant. The addition of FHA failed to increase (it even slightly decreased) the intrinsic kinase activity of $PknB_{CD}$ or $PknB_{CD,L33E}$ toward the peptide substrate (Fig. 2F), indicating that the FHA domain of GarA does not function as an allosteric kinase activator. Together, the above crystallographic and enzymatic results therefore imply that, in the case of GarA, the phosphorylated activation loop of PknB serves as a docking (phospho)site for substrate recruitment.

The downstream phospho-independent complex GarA-ODH

In Actinobacteria, the catalytic domains of components E1o (ODH) and E2o (dihydrolipoamide succinyl transferase) of the ODH complex (homologs of *Escherichia coli* SucA and SucB, respectively) are encoded in a single polypeptide, named OdhA in Corynebacteriaceae (*33*) and KGD in Mycobacteriaceae (*34*). E1o (SucA) is a thiamin diphosphate–dependent enzyme that, in addition to its ODH activity (EC 1.2.4.2) as part of the ODH complex, also exhibits 2-oxoglutarate decarboxylase (EC 4.1.1.71) and 2-oxoglutarate:glyoxylate carboligase (EC 2.2.1.5) activities (*21*, *34*–*36*). In previous work, we characterized the crystal structure of *M. smegmatis* KGD (*21*, *37*) and demonstrated that GarA inhibited the E1o domain, corresponding to KGD residues 361 to 1227 ($KGD_{Δ360}$) (*21*). To gain insight into the mode of phospho-independent recognition and inhibition of KGD, we crystallized $KGD_{Δ360}$ in complex with the FHA domain of GarA ($GarA_{Δ44}$) (table S1). *M. smegmatis* proteins were used, but we maintained *M. tuberculosis* residue numbering for GarA to allow comparison with

the $PknB_{CD}$-GarA complex [the two mycobacterial GarA homologs are 95% identical (see fig. S1), including all residues involved in protein-protein interactions].

The FHA domain of GarA bound to the $KGD_{\Delta 360}$ homodimer with a 2:2 stoichiometry (Fig. 3A). FHA binding promoted no major conformational changes in $KGD_{\Delta 360}$, because the overall root mean square deviation (RMSD) between the holo [Protein Data Bank (PDB) code 2YIC] and FHA-bound structures of wild-type $KGD_{\Delta 360}$ was 0.43 Å for 811 Cα atoms. In addition, the structure of the *M. smegmatis* FHA domain was structurally identical to that of the PknB-bound *M. tuberculosis* FHA domain, with an overall RMSD of 0.3 Å for 90 equivalent Cα atoms. The apical binding surface of the FHA domain was in contact with a strand-connecting loop (residues 586 to 594) and two outer α helices (residues 475 to 500 and 785 to 813) of KGD, ~30 Å away from the catalytic center. The protein-protein interaction buried ~2000 $Å^2$ of the molecular surfaces and was stabilized through hydrophobic and polar contacts, including several intermolecular salt bridges and hydrogen-bonding interactions (Fig. 3B). Partially mimicking a phosphorylated residue, the Asp^{795} carboxylate from KGD outer helix 785–813 occupied the phosphate-binding pocket

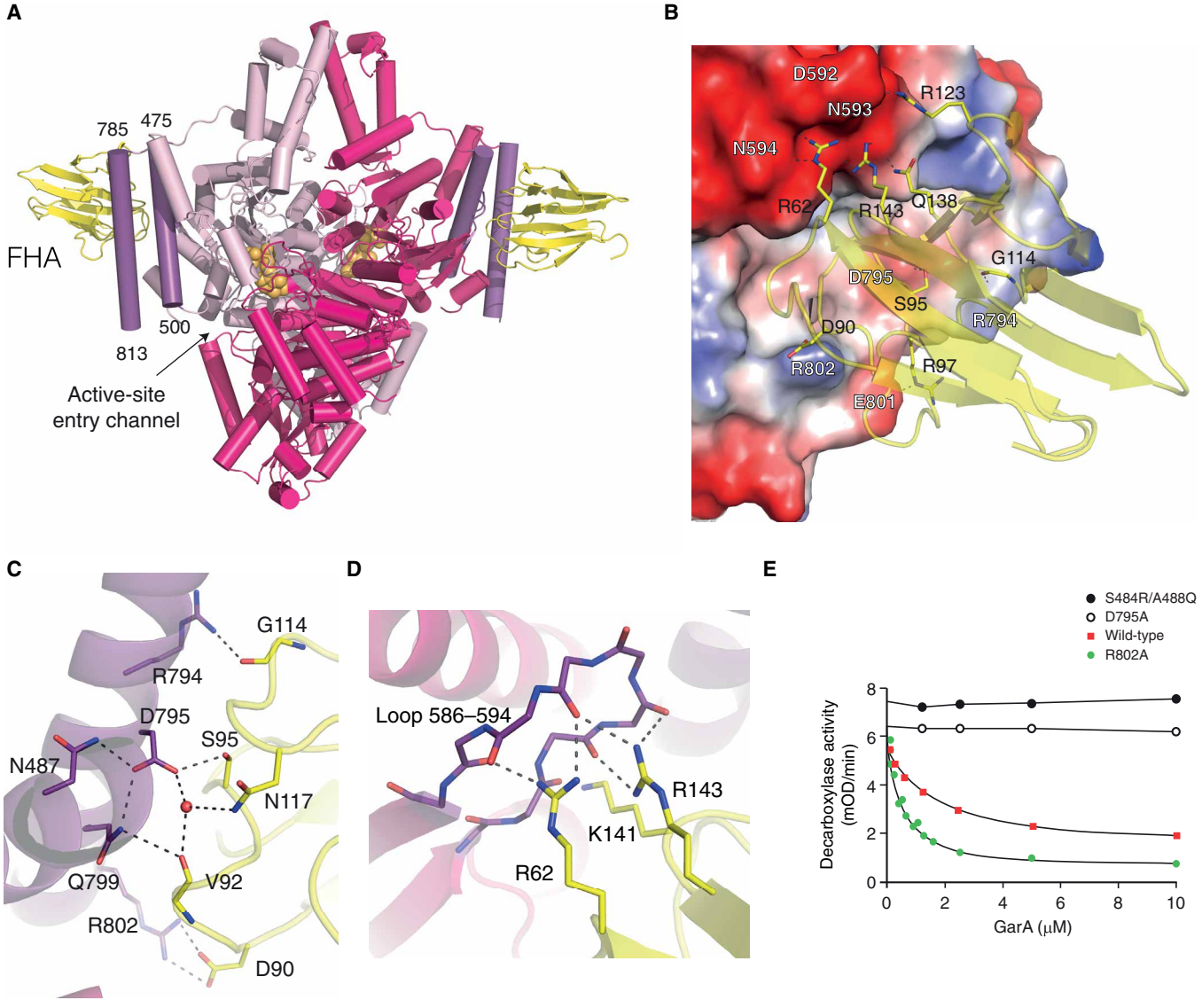

Fig. 3. Structure of the GarA FHA domain ($GarA_{\Delta 44}$)–E1o ($KGD_{\Delta 360}$) complex. (**A**) Crystal structure of the GarA FHA domain ($GarA_{\Delta 44}$) bound to the E1o domain of KGD ($KGD_{\Delta 360}$). Two GarA FHA domain molecules (yellow) bind the outer helices, 475–500 and 785–813 (purple), of the E1o homodimer (magenta). The cofactor thiamine diphosphate (ThDP) at the E1o active site is shown in sphere representation (orange). (**B**) Overall view of the protein-protein interface, showing the molecular surface of KGD color-coded according to electrostatic charge, and GarA FHA domain in ribbon representation. The electrostatic surface is represented color-coded from acidic (red) to basic (blue). All protein residues involved in intermolecular hydrogen bonds are labeled (black label for GarA residues and white labels for surface KGD residues). (**C**) Close-up view of the pThr-binding pocket showing atomic interactions of the phosphomimetic residue Asp^{795} in KGD. Color-coding as in (A). (**D**) Hydrogen bonds between GarA FHA domain Arg^{62} and Arg^{143} (yellow) and main-chain carbonyl groups from the KGD loop 586–594 (in violet, side chains are omitted for clarity). (**E**) Catalytic activity of wild-type $KGD_{\Delta 360}$ (red squares) and three interface mutants: D795A (black open circles), S484R/A488Q (black filled circles), and R802A (green circles) in the presence of the GarA FHA domain. Values are the mean of three independent measurements ($n = 3$); SEM values (not shown) are in the range from 0.1 to 0.5.

of the FHA domain (Fig. 3C), where it made a hydrogen bond with the hydroxyl group of GarA Ser^{95}, a crucial pThr-interacting residue. Two other side chains from the same KGD helix, Arg^{794} and Gln^{799}, were hydrogen-bonded to the backbone carbonyls of GarA residues Gly^{114} and Val^{92}, respectively, and further stabilized the observed orientation of the helix across the pThr-binding pocket. On the other half of the interface, the KGD loop 586–594 was tightly held in place through several hydrogen-bonding interactions of its backbone carbonyl groups with the guanidinium groups of residues Arg^{62} and Arg^{143} from the FHA domain (Fig. 3D).

The observed GarA-KGD interface is similar to a model proposed for the homologous OdhA-OdhI complex from *C. glutamicum* (*38*) and can account for the results of the OdhA-OdhI cross-linking experiments reported in that study. To further validate the observed interface, we produced three KGD surface mutants: (i) substitution of the charged residue Asp^{795} that mimics the phosphorylated residue with alanine (D795A); (ii) substitution of two residues involved in the interface, Ser^{484} and Ala^{488}, with arginine and glutamine, respectively (S484R, A488Q), to prevent formation of a stable complex by adding two bulky side chains; and (iii) substitution of the basic residue Arg^{802}, engaged in an intermolecular salt bridge, with alanine (R802A). These mutants retained wild-type decarboxylase activity but differed in their interaction with GarA. Mutants $KGD_{\Delta360,D795A}$ and $KGD_{\Delta360,S484R,A488Q}$ were not inhibited by GarA, even at high concentrations (Fig. 3E), likely because the mutations precluded FHA binding. These results highlight the functional importance of the phosphomimetic Asp^{795} carboxylate and the primary role of the FHA phosphate–binding pocket in phospho-independent KGD recognition. In contrast, $KGD_{\Delta360,R802A}$ was more efficiently inhibited by GarA (Fig. 3E) than was the wild-type enzyme. The inhibition constant K_i was displaced from 2.5 μM for wild-type $KGD_{\Delta360}$ to 0.4 μM for $KGD_{\Delta360,R802A}$. The crystal structure of this KGD point mutant in complex with GarA (table S1) revealed that the absence of the Arg^{802} side chain allowed a rotation of 7° of the KGD helix 785–813 with respect to the GarA phosphate–binding pocket, optimizing protein-protein interactions that presumably compensate for the loss of the intermolecular salt bridge. In agreement with this observation, *C. glutamicum* OdhA has a small side chain (serine) at the equivalent position of KGD Arg^{802} and is more efficiently inhibited by OdhI (*23*), with a K_i 100-fold lower than that of GarA for KGD in *M. smegmatis*.

Dynamic allosteric inhibition of the ODH

GarA binding to a distal region does not block substrate access to the active site, nor does it promote structural changes in KGD. What then is the mode of action of GarA as a KGD inhibitor? Our previous structural and mutagenesis studies of mycobacterial KGD (*21*, *37*) revealed that formation of the post-decarboxylation covalent reaction intermediate triggered important conformational changes, most notably a global rearrangement of the active-site environment that creates a binding funnel for the acceptor substrate(s). These concerted protein motions promote the transition from a basal resting state of KGD to a fully active state (*39*) and are intimately linked to a ~4 Å shift of a surface-exposed α helix (residues 785 to 813). It is precisely this α helix that lies at the center of the GarA-binding interface and contains the phosphomimetic residue Asp^{795} (Fig. 3A). Therefore, formation of the GarA-KGD complex locks the enzyme in its basal resting state by blocking the helical movement and the ensuing structural transition.

Our structural studies of KGD had shown that formation of the post-decarboxylation covalent intermediate can be achieved in the initial resting conformation, before the structural transition occurs (*37*), and therefore should not be affected by GarA binding. To further investigate this hypothesis, we soaked crystals of the $KGD_{\Delta360,R802A}$-$GarA_{\Delta44}$ complex for long periods of time in 2-oxoglutarate. The crystal structure, refined at 2.4 Å resolution (table S1), showed no major conformational changes in the active site, indicating that the structural transition had not taken place. However, the post-decarboxylation covalent intermediate derived from 2-oxoglutarate was clearly visible in the electron density maps (fig. S7), demonstrating that GarA binding did not prevent the first reaction step. These results further confirm our proposed inhibition mechanism based on blocking protein motions and are consistent with previous circular dichroism studies of *M. tuberculosis* KGD, indicating that GarA inhibited the second half of the enzymatic reaction (*39*).

Moreover, GarA would be expected to have a differential effect on the reported KGD catalytic activities. By stabilizing the basal conformation of KGD, GarA binding precludes formation of the acceptor substrate-binding sites for the lipoyl and glyoxylate groups needed to complete the dehydrogenase and carboligase reactions, respectively. In contrast, the semialdehyde species in the decarboxylation reaction is generated by direct proton attack to the post-decarboxylation covalent intermediate and should therefore be less affected by GarA. In agreement with this model, at 5 μM concentration, GarA efficiently inhibited the dehydrogenase reaction (no ODH activity could be detected) but did not totally abolish the decarboxylase reaction, because a residual succinic-semialdehyde production (~27% of the value in the absence of GarA) was measured for $KGD_{\Delta360}$ under the same conditions (*40*). Together, the above results demonstrate that nonphosphorylated GarA modulates KGD activity through a dynamic allosteric inhibition mechanism.

Structural basis of FHA-protein interactions

The structures of the phosphorylation-dependent (upstream) and phosphorylation-independent (downstream) GarA complexes described above revealed that, despite the considerable differences in the target proteins, the FHA domain retained its structural integrity and engaged essentially the same molecular surface for protein binding. In the two protein complexes, the interface included the FHA phosphate–binding pocket, defined by the C terminus of strand β3 and the loops β4-β5 and β6-β7, and a shallow adjacent cleft of positively charged residues from loops β1-β2 and β10-β11. As shown by NMR studies of the autoinhibited, closed form of GarA (*13*), this same interface was also used for self-recognition of $pThr^{22}$ (Fig. 4, A to C). The dual binding specificity of GarA toward phosphorylated and nonphosphorylated proteins is intriguing. Guided by the available structures, we performed surface plasmon resonance (SPR) experiments to explore the effect of four *M. smegmatis* GarA mutations within the common interface: one involving a central pThr-binding residue, Ser^{95} (S95A), and three others involving positively charged residues from the adjacent region, Arg^{62}, Lys^{141}, and Arg^{143} (R62A, L151E, and R143A) (Figs. 2 and 3).

Our structures and mutational studies underscore the importance of the PknB $pThr^{171}$ interaction within the GarA phosphate–binding pocket as a primary determinant of PknB binding. Similarly, the interactions of KGD Asp^{795}, which mimics pThr, are essential for KGD binding. Mutation of the conserved GarA Ser^{95} in the phosphate-binding site completely abolished the $PknB_{CD}$-GarA interaction (Table 1), in full agreement with previous observations that GarA was unable to interact with the nonphosphorylated forms

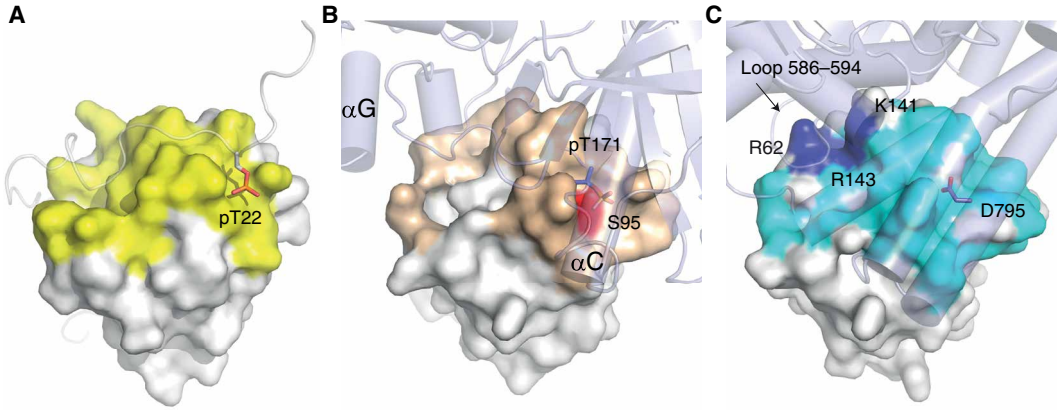

Fig. 4. Dual binding specificity of the GarA FHA domain. The same region of the GarA FHA domain (colored molecular surface) mediates both phosphorylation-dependent and phosphorylation-independent interactions with binding partners. The structures shown are those of (**A**) the closed conformation of autoinhibited GarA, (**B**) the GarA-PknB$_{CD,L33A}$ complex, and (**C**) the GarA$_{\Delta 44}$-KGD$_{\Delta 360}$ complex. The FHA domain is shown in a similar orientation in each complex.

Table 1. Binding affinities of KGD$_{\Delta 360}$ and PknB$_{CD}$ for GarA point mutants. The binding affinities of *M. tuberculosis* PknB catalytic domain (*Mt*PknB$_{CD}$) and *M. smegmatis* KGD (Ms KGD$_{\Delta 360}$) for different *Ms*GarA point mutants were determined by SPR. Values represent $K_D \pm$ SE from a representative experiment (fig. S8) of three or more independent experiments. n.d., not determined (no reliable fit).

GarA	KGD K_D (μM)	PknB$_{CD}$ K_D (μM)
Wild type	1.92 ± 0.15	12.2 ± 1.0
R62A	n.d.	14.7 ± 1.5
S95A	1.89 ± 0.11	n.d.
K141E	n.d.	10.8 ± 0.8
R143A	n.d.	12.4 ± 1.1

of PknB and PknG (*18*, *20*). However, the same GarA substitution, S95A, had no effect on the KGD dissociation constant (Table 1 and fig. S8B). This last result is consistent with a previous observation that this mutation does not affect KGD inhibition (*13*) but seems to contradict the essentiality of phosphomimetic KGD Asp^{795} (Fig. 3, C and E). This apparent discrepancy is probably due to a distinct pattern of interactions involving the Asp^{795} carboxylate (compared to a pThr residue) in the phosphate-binding pocket. The carboxylate group is hydrogen-bonded to the hydroxyl group of Ser^{95} and to a water molecule, which, in turn, makes strong hydrogen bonds with Asn^{117} and main-chain backbone atoms of GarA (Fig. 3C). Because it disrupts the whole hydrogen-bonding network, the substitution of KGD Asp^{795} (D795A) is therefore expected to have a stronger effect on the binding energy than that of GarA Ser^{95} (S95A).

In addition to the dissimilarities in the phosphate-binding pocket (occupation by pThr versus Asp), the PknB$_{CD}$-GarA and GarA-KGD complexes also differ in the interactions on the positively charged face of the FHA domain: substitutions of the GarA basic residues R62A, K141E, or R143A in the loops β1-β2 and β10-β11 had little or no effect on the PknB$_{CD}$ binding affinity (Table 1 and fig. S8A). In contrast, these same substitutions were found to considerably affect KGD binding (Table 1), because the basic residues make several ionic interactions with the KGD loop 586–594 (Fig. 3D). In summary, the above observations suggest that recognition of KGD is driven by extensive interactions, not only with the phosphate-binding pocket but also with the adjacent basic cleft of GarA, which are required to efficiently block KGD protein motions during catalysis, whereas recognition of autophosphorylated PknB [or the GarA N-terminal phosphopeptide in the autoinhibited closed form (*12*, *13*)] is dominated by interactions of the pThr residue with the canonical phosphate-binding pocket of GarA.

DISCUSSION

FHA domains are the only type of eukaryotic-like phosphoresidue-binding protein modules so far identified in bacteria, where they fulfill important albeit poorly characterized roles. For instance, in *M. tuberculosis*, at least five FHA domain–containing proteins have been reported to participate in the STPK-mediated control of essential biological processes such as cell wall synthesis (*14*, *41*), cell division (*42*), and central metabolism (*18*). In particular, the GarA-mediated control of a crucial node at the crossroads of carbon and nitrogen metabolism, conserved in and restricted to Actinobacteria (Fig. 1B), arguably represents the bacterial FHA domain–mediated signaling pathway with the most complete molecular description so far. Together with previous studies on mycobacterial GarA and corynebacterial OdhI (*13*, *18*, *19*, *22*–*25*), our results substantially broaden the known functional versatility of the FHA domain beyond that of a simple pThr-recognition module in cell signaling. In particular, the structures of the upstream and downstream GarA complexes demonstrate how a single FHA domain protein can engage its canonical phosphate-binding pocket in biologically relevant, specific, phosphorylation-dependent as well as phosphorylation-independent, protein-protein interactions (Fig. 4). Moreover, the same binding region of the FHA domain is likely involved in the interaction of GarA with at least two other metabolic, structurally unrelated enzymes, because the amino acid substitutions S95A in the phosphate-binding pocket and K141E in the adjacent basic region abolish GarA binding and regulation of glutamate synthase and NAD-dependent GDH in mycobacteria (*13*).

This dual binding specificity of the GarA FHA domain can be partially accounted for by phosphate mimicry of KGD Asp^{795}, which is crucial for complex formation and occupies the phosphate-binding pocket. Aspartate and glutamate are frequently used as "phosphomimetic"

residues to probe the constitutively phosphorylated state in protein phosphoregulation studies and even for structural studies (*43*, *44*). Although in some cases it has been suggested that phosphomimetic mutations might enhance FHA binding (*45*–*47*), there had been no previous structural evidence for this, and extensive published studies have instead suggested that phosphomimetic residues might not fit into the binding site of FHA domains or other adaptor proteins [reviewed in (*48*) and references therein]. Here, the structure of the GarA-KGD complex illustrates a clear example of functional, naturally occurring phosphomimetics. The carboxylate group of KGD Asp^{795}, a residue essential for complex formation with GarA, occupies a similar position as the pThr side chain in the PknB-GarA complex, with a water molecule filling the cavity left by the missing oxygen atoms of the phosphate to partially restore the hydrogen-bonding network (Fig. 3C). These observations demonstrate that phosphomimetic recognition by FHA domains is possible, although in this case we should emphasize that it is favored by additional protein-protein interactions outside the phosphate-binding pocket.

In addition to contributing to a better understanding of the GarA-mediated signaling pathway at the molecular level, the individual crystal structures reported here raise important mechanistic issues. For example, the role of protein dynamics in enzyme function remains poorly understood or difficult to interpret (*49*). Previously published crystal structures of KGD (*21*, *37*) stressed the importance of protein motions for efficient catalysis and regulation, and that of the GarA-KGD complex now illustrates a potential approach for using dynamics to modulate function (*50*) and eventually to design efficient enzyme inhibitors. On the other hand, the structure of the PknB-GarA complex raises puzzling questions on the kinase activation mechanism. Phosphorylation of the activation loop is a hallmark of the active state for many serine-threonine protein kinases (*32*, *51*), because it usually leads to conformational changes required for catalysis (*52*). In PknB, phosphorylation of two Thr residues in the activation loop is also required for full kinase activity (*53*), but the structural and activity studies reported above suggest that the interaction between the pThr residues and the HRD motif is not required to achieve a catalytically competent active site. Instead, it appears that phosphorylation of the activation loop serves to generate a docking site for FHA domain–mediated GarA recruitment, which accounts for the high kinase activity toward this particular substrate. Further experiments are required to elucidate the molecular mechanisms underpinning kinase activation against other PknB substrates.

In summary, the work reported here revealed structural snapshots of a single FHA domain protein caught in upstream and downstream protein-protein complexes, providing important insights not only into the functional adaptability of these domains in bacterial signaling but also into kinase activation and unanticipated allosteric dynamic mechanisms of metabolic regulation.

MATERIALS AND METHODS

Reagents

The synthetic 17-mer peptide SDEVTVETTSVFRADFL, corresponding to residues 14 to 30 of *M. tuberculosis* GarA (*Mt*GarA), was purchased from Thermo Fisher Scientific (purity, >98%).

Cloning and mutagenesis

Genes were amplified by polymerase chain reaction from genomic DNA of *M. smegmatis* mc^2 155 (MSMEG_5049 for *kgd*, MSMEG_3647 for *garA*, MSMEG_4283 for *dlaT*, and MSMEG_0903 for *lpdA*) and *M. tuberculosis* H37Rv (Rv0014c for *pknB*, Rv0243c for *gabD1*, and Rv1827 for *garA*) and cloned into pET-28a (Novagen) or pDEST17 (Invitrogen), as previously described (*21*, *26*, *28*). Site-directed mutagenesis was performed on pET28a-*Mt*$PknB_{CD}$ (L33E), pET28a-*Ms*$KGD_{\Delta360}$ (R802A, D795A, S484R/A488Q), and pET28a-*Ms*GarA (R62A, S95A, K141E, R143A). All plasmids were verified by DNA sequencing.

Protein production

The recombinant proteins *Ms*KGD, *Ms*$KGD_{\Delta360}$, *Ms*GarA, *Ms*DlaT, *Ms*Lpd, *Mt*GabD1, and *Mt*GarA and the two FHA domains alone (*Ms*$GarA_{\Delta44}$ used in cocrystallization with $KGD_{\Delta360}$ and *Mt*$GarA_{\Delta43}$ used for kinase assays) were overproduced in *E. coli* and purified as previously described (*21*, *26*). *Ms*GarA and its mutant versions were also produced in microfermentor units, following established protocols (*54*). *Mt*$PknB_{1–279}$ (referred to as $PknB_{CD}$) and its mutant version carrying the substitution L33E ($PknB_{CD,L33E}$) were expressed for 15 hours at 22°C with 100 μM isopropyl-β-D-thiogalactopyranoside (IPTG). Both proteins were purified using the same protocol. *E. coli* cells were harvested by centrifugation, resuspended in lysis buffer [50 mM NaH_2PO_4 (pH 8), 500 mM NaCl, 5% glycerol, 25 mM imidazole, and 1 mM dithiothreitol (DTT)] supplemented with cOmplete protease inhibitor cocktail (Roche) and sonicated. After centrifugation, the supernatant was loaded onto a 5-ml HisTrap HP column (GE Healthcare), and the His-tagged protein was purified by applying a linear imidazole gradient (25 to 500 mM). Next, the His_6 tag was removed by incubating for 18 hours at 18°C in the presence of His_6-tagged Tobacco Etch Virus (TEV) protease (*55*) at a 1:30 ratio (w/w) in buffer [25 mM Hepes (pH 8), 150 mM NaCl, 5% glycerol, and 1 mM DTT] followed by separation on a Ni-nitrilotriacetic acid (NTA) agarose column (Qiagen). Then, the protein was further purified by size exclusion chromatography on a Superdex 200 column (GE Healthcare) equilibrated in 25 mM Hepes (pH 8), 150 mM NaCl, 5% glycerol, and 1 mM DTT. Fractions corresponding to the PknB peaks, as confirmed by SDS-polyacrylamide gel electrophoresis, were later pooled and concentrated up to 40 mg/ml, flash-frozen in liquid nitrogen, and stored at −80°C. All proteins were quantified using the molar absorption coefficient predicted from the amino acid sequence by the ProtParam tool (http://web.expasy.org/protparam/).

Enzyme activity assays

Kinase activity assays were performed in 96-well plates. Each activity measurement was performed in a final volume of 20 μl, containing 50 mM tris-HCl (pH 7.4), 0.1% (v/v) 2-mercaptoethanol, 0.01% (v/v) Brij-35, 2 mM $MnCl_2$, 100 μM [γ-^{32}P]ATP [5 to 50 counts per minute (cpm)/pmol], and 330 μM 17-mer peptide or 25 μM *Mt*GarA as substrate. In addition, the kinase assays shown in Fig. 2F were done in the absence or presence of 92 μM *Mt*$GarA_{\Delta43}$. The enzyme concentration in the assays was 0.2 to 5 μM and 3 to 12 nM when using the 17-mer peptide or *Mt*GarA as substrates, respectively. The kinase reactions were started by the addition of 4 μl [γ-^{32}P]ATP-Mn^{+2} and were performed at room temperature. The reactions were stopped by the addition of phosphoric acid, and 4 μl of each reaction was spotted on P81 phosphocellulose papers (Whatman) using the epMotion 5070 (Eppendorf) workstation. The papers were washed in 0.01% phosphoric acid, dried, and then measured and analyzed using a PhosphorImager (FLA-9000 Starion, Fujifilm). Each reaction was performed in duplicate (<10% variation), and each assay was performed

at least twice (<20% variation). In all cases, specific activity values were derived from reactions performed using three different enzyme concentrations within the indicated ranges (<20% variation), verifying a linear dependence of activity with kinase concentration. The proportion of 17-mer peptide or *Mt*GarA consumed in the reactions was lower than 10% and 30%, respectively. *Mt*GarA consumption was verified to be linear in time up to 50% its initial concentration. Under the experimental conditions used to test phosphorylation of the 17-mer peptide or *Mt*GarA, $PknB_{CD}$ or $PknB_{CD,L33E}$ autophosphorylation represented less than 5% of the total signal. The measured signal was at least five times higher than the lecture on the background.

Determinations of 2-oxoglutarate decarboxylase and ODH activities were carried out as previously described (*21*). Briefly, for the decarboxylase activity, reactions contained 2 μM $MsKGD_{\Delta360}$, 1 to 3 mM 2-oxoglutarate, 0.2 mM ThDP, 1 mM $MgCl_2$, 0.55 to 1.1 μM *Mt*GabD1, and 1 to 2 mM $NADP^+$ (nicotinamide adenine dinucleotide phosphate) in 50 mM potassium phosphate (pH 6.5). Reactions were started by the addition of 2-oxoglutarate at 37°C, and initial rates were calculated during the linear phase of the reaction (10 to 20 min) following 340-nm absorbance using a microplate reader. For measuring ODH activity, the reaction contained 1 to 3 mM 2-oxoglutarate, 1 mM CoA-SH, 0.2 mM ThDP, 1 mM $MgCl_2$, 2 μM *Ms*KGD, 4 μM *Ms*DlaT, 0.5 μM *Ms*Lpd, and 1 to 2 mM 3-acetylpyridine dinucleotide ($AcNAD^+$) in 50 mM potassium phosphate (pH 6.5). $AcNAD^+$ was used instead of NAD^+ to prevent enzyme inhibition by NADH (reduced form of NAD^+). Reactions were started by the addition of 2-oxoglutarate at 37°C, and initial rates were calculated during the linear phase of the reaction (10 to 20 min). When required, *Ms*GarA was diluted in phosphate-buffered saline (PBS) and added to a final concentration ranging from 0.02 to 10 μM, and AcCoA to a final concentration ranging from 0.01 to 4 mM. The rate of $AcNAD^+$ reduction was calculated by spectrophotometry based on the absorption coefficient of $AcNADH,H^+$ ($\varepsilon_{340nm} = 6220\ M^{-1}\ cm^{-1}$). When appropriate, *Ms*GarA was diluted in PBS and added to the assay mixture at 5 μM, unless otherwise stated. Experiments were performed in triplicate.

Isothermal titration calorimetry

*Mt*GarA binding to $PknB_{CD}$ or $PknB_{CD,L33E}$ was assayed using a high-precision VP-ITC system (MicroCal Inc.) with the following parameters: the isothermal titration calorimetry (ITC) cell (1.4 ml) contained 10 μM *Mt*PknB, preincubated with 2 μM ATP in 25 mM Hepes (pH 7.5), 150 mM NaCl, and 1 mM DTT, and the syringe (150 μl) contained 250 μM *Mt*GarA in the same buffer. Sample solutions were thoroughly degassed under vacuum, and each titration was performed at 15°C by injections of 10 μl every 210 s using a 290 rpm rotating syringe. Raw heat signal collected with a 16-s filter was corrected for the dilution heat and normalized to the concentration of ligand injected. Data were fit to a bimolecular model using the Origin software provided by the manufacturer. The ITC experiments were performed at least twice to ensure reproducibility. A representative experiment is shown in fig. S3, from which the reported thermodynamic parameters have been calculated.

Analytical ultracentrifugation

Sedimentation coefficients were determined at 20°C, using a Beckman Coulter XL-I centrifuge equipped with an AN60-Ti rotor equipped with Rayleigh interference detection. Samples were centrifuged for 17 hours at 42,000 rpm, and profiles were recorded every 5 min. Sedimentation scans were analyzed by the continuous size distribution procedure c(S) with the program Sedfit 15.01 (*56*). All c(S) distributions were calculated with a fitted frictional ratio f/f0 and a maximum entropy regularization procedure with a confidence level of 0.68. Theoretical sedimentation coefficients were calculated from the atomic coordinates using HYDROPRO (*57*) and compared to the experimental sedimentation coefficients obtained from ultracentrifugation analysis.

Surface plasmon resonance

SPR measurements were performed at 25°C on an NTA sensor chip using a Biacore 2000 instrument (GE Healthcare) equilibrated with 25 mM Hepes (pH 8), 150 mM NaCl, 50 μM EDTA, and 0.005% Tween 20 (running buffer). The sensor chip was activated by injecting 0.5 mM $NiCl_2$ followed by the capture of the His-tagged proteins *Ms*KGD full length and $MtPknB_{CD}$ on two independent channels. The reference flow cell was prepared by the same procedure in absence of protein. Various concentrations of wild-type *Ms*GarA, or the single-point mutants R61A, S94A, K140E, and R142A (referred to in the text as R62A, S95A, K141E, and R143A, respectively, to maintain consistency with *Mt*GarA residue numbering), were injected onto the surfaces at a flow rate of 50 μl min^{-1}, and the binding signals were monitored. Protein dissociation was realized by injecting the running buffer, and the surface was regenerated by injecting 0.25 M imidazole followed by 0.35 M EDTA and 0.1% SDS before the next cycle. Control flow cell sensorgrams were subtracted from the ligand flow cell sensorgrams, and averaged buffer injections were subtracted from analyte sensorgrams. Response at equilibrium (Req) was obtained directly from the plateau region of the sensorgrams. The saturation curves obtained by plotting Req versus the analyte concentration were fitted with a steady-state model to obtain the apparent equilibrium dissociation constant K_D, using the BIAevaluation 4.2 software (GE Healthcare).

Crystallization and data collection

Crystallization screenings were carried out using the sitting-drop vapor diffusion method and a Mosquito nanoliter-dispensing crystallization robot (TTP Labtech); hits were improved by handmade hanging drops in 24-well plates at the same temperature. Optimized conditions for crystal growth of the different protein complexes (protein concentrations of 20 to 25 mg/ml, molar ratio of 1:1) are as follows: (i) $MtPknB_{L33E}$-*Mt*GarA: 100 mM Hepes, 4% (w/v) PEG400 (polyethylene glycol, molecular weight 400), 2 M $(NH_4)_2SO_4$, and 4 mM AMP-PCP (pH 7.5); (ii) $MsKGD_{\Delta360}$-$MsGarA_{\Delta44}$: 50% 2-methyl-2,4-pentanediol (MPD), 100 mM MES, 2 mM ThDP, and 5 mM $MgCl_2$ (pH 6.5); and (iii) $MsKGD_{\Delta360,R802A}$-$MsGarA_{\Delta44}$: 47% MPD, 100 mM Na Hepes, 2 mM ThDP, and 5 mM $MgCl_2$ (pH 7.5). The enamine-ThDP reaction intermediate for KGD in the presence of GarA was obtained by soaking crystals of the $MsKGD_{\Delta360,R802A}$-$MsGarA_{\Delta44}$ (grown as described above) with 20 mM 2-oxoglutarate for 8 min before freezing.

X-ray diffraction data were collected from single crystals at 100 K using synchrotron radiation at beamlines Proxima 1 (Synchrotron Soleil, Saint-Aubin, France) and ID14-1 (ESRF, Grenoble, France). Data processing was carried out with programs XDS (*58*) and AIMLESS (*59*).

Structure determination and refinement

The crystal structures of all protein complexes were solved by molecular replacement techniques using either the *Mt*PknB catalytic domain (PDB code 1O6Y) or the apo form of $MsKGD_{\Delta360}$ (PDB code 2YIC)

as search probes with the program PHASER (*60*). The bound FHA domain in all structures, as well as the cofactor ThDP (for the KGD complexes) or the nucleotide AMP-PCP (for the PknB complex), was clearly visible in Fourier difference maps and could be manually traced during refinement. All crystallographic models were refined through iterative cycles of manual model building with COOT (*61*) and reciprocal space refinement with BUSTER (*62*). Because of important conformational changes in the PknB kinase core, the entire N-lobe was removed during the first refinement rounds and gradually rebuilt through iterative cycles of refinement and manual model building. The structure was validated through the MolProbity server (http://molprobity.biochem.duke.edu). Figures were generated and rendered with PyMOL 1.5.0.2 (Schrödinger LLC).

SUPPLEMENTARY MATERIALS

stke.sciencemag.org/cgi/content/full/12/580/eaav9504/DC1
Fig. S1. Alignment of GarA homologs in selected Actinobacteria.
Fig. S2. Continuous sedimentation coefficient distribution analysis of the $PknB_{CD}$-GarA complex.
Fig. S3. ITC characterization of the interaction between autophosphorylated $PknB_{CD}$ and GarA.
Fig. S4. The N-terminal GarA extension occupies a similar position in different GarA structures.
Fig. S5. Conserved mode of phosphopeptide recognition in different *M. tuberculosis* FHA domains.
Fig. S6. Detailed structure of the PknB activation loop bound to GarA.
Fig. S7. Formation of the enamine-ThDP covalent adduct in the presence of GarA.
Fig. S8. SPR studies of protein-protein interactions.
Table S1. Data collection and refinement statistics.
References (*64*, *65*)

REFERENCES AND NOTES

1. A. Wehenkel, M. Bellinzoni, M. Graña, R. Duran, A. Villarino, P. Fernandez, G. André-Leroux, P. England, H. Takiff, C. Cerveñansky, S. T. Cole, P. M. Alzari, Mycobacterial Ser/Thr protein kinases and phosphatases: Physiological roles and therapeutic potential. *Biochim. Biophys. Acta* **1784**, 193–202 (2008).
2. S. F. F. Pereira, L. Goss, J. Dworkin, Eukaryote-like serine/threonine kinases and phosphatases in bacteria. *Microbiol. Mol. Biol. Rev.* **75**, 192–212 (2011).
3. A. Kobir, L. Shi, A. Boskovic, C. Grangeasse, D. Franjevic, I. Mijakovic, Protein phosphorylation in bacterial signal transduction. *Biochim. Biophys. Acta* **1810**, 989–994 (2011).
4. B. T. Seet, I. Dikic, M.-M. Zhou, T. Pawson, Reading protein modifications with interaction domains. *Nat. Rev. Mol. Cell Biol.* **7**, 473–483 (2006).
5. J. Jin, T. Pawson, Modular evolution of phosphorylation-based signalling systems. *Philos. Trans. R. Soc. B Biol. Sci.* **367**, 2540–2555 (2012).
6. I. Sadowski, J. C. Stone, T. Pawson, A noncatalytic domain conserved among cytoplasmic protein-tyrosine kinases modifies the kinase function and transforming activity of Fujinami sarcoma virus P130gag-fps. *Mol. Cell. Biol.* **6**, 4396–4408 (1986).
7. M. Pallen, R. Chaudhuri, A. Khan, Bacterial FHA domains: Neglected players in the phospho-threonine signalling game? *Trends Microbiol.* **10**, 556–563 (2002).
8. K. Hofmann, P. Bucher, The FHA domain: A putative nuclear signalling domain found in protein kinases and transcription factors. *Trends Biochem. Sci.* **20**, 347–349 (1995).
9. A. Mahajan, C. Yuan, H. Lee, E. S.-W. Chen, P.-Y. Wu, M.-D. Tsai, Structure and function of the phosphothreonine-specific FHA domain. *Sci. Signal.* **1**, re12 (2008).
10. J. Li, G. P. Smith, J. C. Walker, Kinase interaction domain of kinase-associated protein phosphatase, a phosphoprotein-binding domain. *Proc. Natl. Acad. Sci. U.S.A.* **96**, 7821–7826 (1999).
11. D. Durocher, S. P. Jackson, The FHA domain. *FEBS Lett.* **513**, 58–66 (2002).
12. P. Barthe, C. Roumestand, M. J. Canova, L. Kremer, C. Hurard, V. Molle, M. Cohen-Gonsaud, Dynamic and structural characterization of a bacterial FHA protein reveals a new autoinhibition mechanism. *Structure* **17**, 568–578 (2009).
13. T. J. Nott, G. Kelly, L. Stach, J. Li, S. Westcott, D. Patel, D. M. Hunt, S. Howell, R. S. Buxton, H. M. O'Hare, S. J. Smerdon, An intramolecular switch regulates phosphoindependent FHA domain interactions in *Mycobacterium tuberculosis*. *Sci. Signal.* **2**, ra12 (2009).
14. C. L. Gee, K. G. Papavinasasundaram, S. R. Blair, C. E. Baer, A. M. Falick, D. S. King, J. E. Griffin, H. Venghatakrishnan, A. Zukauskas, J.-R. Wei, R. K. Dhiman, D. C. Crick, E. J. Rubin, C. M. Sassetti, T. Alber, A phosphorylated pseudokinase complex controls cell wall synthesis in Mycobacteria. *Sci. Signal.* **5**, ra7 (2012).
15. Y. Tong, W. Tempel, H. Wang, K. Yamada, L. Shen, G. A. Senisterra, F. MacKenzie, A. H. Chishti, H.-W. Park, Phosphorylation-independent dual-site binding of the FHA domain of KIF13 mediates phosphoinositide transport via centaurin alpha1. *Proc. Natl. Acad. Sci. U.S.A.* **107**, 20346–20351 (2010).
16. A. W. Almawi, L. A. Matthews, Larasati, P. Myrox, S. Boulton, C. Lai, T. Moraes, G. Melacini, R. Ghirlando, B. P. Duncker, A. Guarné, 'AND' logic gates at work: Crystal structure of Rad53 bound to Dbf4 and Cdc7. *Sci. Rep.* **6**, 34237 (2016).
17. M. Bott, Offering surprises: TCA cycle regulation in *Corynebacterium glutamicum*. *Trends Microbiol.* **15**, 417–425 (2007).
18. H. M. O'Hare, R. Durán, C. Cerveñansky, M. Bellinzoni, A. M. Wehenkel, O. Pritsch, G. Obal, J. Baumgartner, J. Vialaret, K. Johnsson, P. M. Alzari, Regulation of glutamate metabolism by protein kinases in mycobacteria. *Mol. Microbiol.* **70**, 1408–1423 (2008).
19. A. E. Belanger, G. F. Hatfull, Exponential-phase glycogen recycling is essential for growth of *Mycobacterium smegmatis*. *J. Bacteriol.* **181**, 6670–6678 (1999).
20. A. Villarino, R. Duran, A. Wehenkel, P. Fernandez, P. England, P. Brodin, S. T. Cole, U. Zimny-Arndt, P. R. Jungblut, C. Cerveñansky, P. M. Alzari, Proteomic identification of *M. tuberculosis* protein kinase substrates: PknB recruits GarA, a FHA domain-containing protein, through activation loop-mediated interactions. *J. Mol. Biol.* **350**, 953–963 (2005).
21. T. Wagner, M. Bellinzoni, A. Wehenkel, H. M. O'Hare, P. M. Alzari, Functional plasticity and allosteric regulation of α-ketoglutarate decarboxylase in central mycobacterial metabolism. *Chem. Biol.* **18**, 1011–1020 (2011).
22. B. Rieck, G. Degiacomi, M. Zimmermann, A. Cascioferro, F. Boldrin, N. R. Lazar-Adler, A. R. Bottrill, F. le Chevalier, W. Frigui, M. Bellinzoni, M.-N. Lisa, P. M. Alzari, L. Nguyen, R. Brosch, U. Sauer, R. Manganelli, H. M. O'Hare, PknG senses amino acid availability to control metabolism and virulence of *Mycobacterium tuberculosis*. *PLOS Pathog.* **13**, e1006399 (2017).
23. A. Niebisch, A. Kabus, C. Schultz, B. Weil, M. Bott, Corynebacterial protein kinase G controls 2-oxoglutarate dehydrogenase activity via the phosphorylation status of the OdhI protein. *J. Biol. Chem.* **281**, 12300–12307 (2006).
24. C. Schultz, A. Niebisch, L. Gebel, M. Bott, Glutamate production by *Corynebacterium glutamicum*: Dependence on the oxoglutarate dehydrogenase inhibitor protein OdhI and protein kinase PknG. *Appl. Microbiol. Biotechnol.* **76**, 691–700 (2007).
25. M. Ventura, B. Rieck, F. Boldrin, G. Degiacomi, M. Bellinzoni, N. Barilone, F. Alzaidi, P. M. Alzari, R. Manganelli, H. M. O'Hare, GarA is an essential regulator of metabolism in *Mycobacterium tuberculosis*. *Mol. Microbiol.* **90**, 356–366 (2013).
26. P. England, A. Wehenkel, S. Martins, S. Hoos, G. André-Leroux, A. Villarino, P. M. Alzari, The FHA-containing protein GarA acts as a phosphorylation-dependent molecular switch in mycobacterial signaling. *FEBS Lett.* **583**, 301–307 (2009).
27. T. Alber, Signaling mechanisms of the *Mycobacterium tuberculosis* receptor Ser/Thr protein kinases. *Curr. Opin. Struct. Biol.* **19**, 650–657 (2009).
28. M. Ortiz-Lombardía, F. Pompeo, B. Boitel, P. M. Alzari, Crystal structure of the catalytic domain of the PknB serine/threonine kinase *fromMycobacterium tuberculosis*. *J. Biol. Chem.* **278**, 13094–13100 (2003).
29. T. A. Young, B. Delagoutte, J. A. Endrizzi, A. M. Falick, T. Alber, Structure of *Mycobacterium tuberculosis* PknB supports a universal activation mechanism for Ser/Thr protein kinases. *Nat. Struct. Biol.* **10**, 168–174 (2003).
30. T. N. Lombana, N. Echols, M. C. Good, N. D. Thomsen, H.-L. Ng, A. E. Greenstein, A. M. Falick, D. S. King, T. Alber, Allosteric activation mechanism of the *Mycobacterium tuberculosis* receptor Ser/Thr protein kinase, PknB. *Structure* **18**, 1667–1677 (2010).
31. A. Wehenkel, P. Fernandez, M. Bellinzoni, V. Catherinot, N. Barilone, G. Labesse, M. Jackson, P. M. Alzari, The structure of PknB in complex with mitoxantrone, an ATP-competitive inhibitor, suggests a mode of protein kinase regulation in mycobacteria. *FEBS Lett.* **580**, 3018–3022 (2006).
32. M. Huse, J. Kuriyan, The conformational plasticity of protein kinases. *Cell* **109**, 275–282 (2002).
33. Y. Usuda, N. Tujimoto, C. Abe, Y. Asakura, E. Kimura, Y. Kawahara, O. Kurahashi, H. Matsui, Molecular cloning of the *Corynebacterium glutamicum* ('*Brevibacterium lactofermentum*' AJ12036) *odhA* gene encoding a novel type of 2-oxoglutarate dehydrogenase. *Microbiology* **142**, 3347–3354 (1996).
34. J. Tian, R. Bryk, M. Itoh, M. Suematsu, C. Nathan, Variant tricarboxylic acid cycle in *Mycobacterium tuberculosis*: Identification of alpha-ketoglutarate decarboxylase. *Proc. Natl. Acad. Sci. U.S.A.* **102**, 10670–10675 (2005).
35. T. Saito, S. Tuboi, Y. Nishimura, G. Kikuchi, On the nature of the enzyme which catalyzes a synergistic decarboxylation of alpha-ketoglutarate and glyoxylate. *J. Biochem.* **69**, 265–273 (1971).
36. L. P. S. de Carvalho, H. Zhao, C. E. Dickinson, N. M. Arango, C. D. Lima, S. M. Fischer, O. Ouerfelli, C. Nathan, K. Y. Rhee, Activity-based metabolomic profiling of enzymatic function: Identification of Rv1248c as a mycobacterial 2-hydroxy-3-oxoadipate synthase. *Chem. Biol.* **17**, 323–332 (2010).
37. T. Wagner, N. Barilone, P. M. Alzari, M. Bellinzoni, A dual conformation of the post-decarboxylation intermediate is associated with distinct enzyme states in mycobacterial KGD (α-ketoglutarate decarboxylase). *Biochem. J.* **457**, 425–434 (2014).
38. K. Raasch, M. Bocola, J. Labahn, A. Leitner, L. Eggeling, M. Bott, Interaction of 2-oxoglutarate dehydrogenase OdhA with its inhibitor OdhI in *Corynebacterium glutamicum*: Mutants and a model. *J. Biotechnol.* **191**, 99–105 (2014).

39. A. Balakrishnan, F. Jordan, C. F. Nathan, Influence of allosteric regulators on individual steps in the reaction catalyzed by *Mycobacterium tuberculosis* 2-hydroxy-3-oxoadipate synthase. *J. Biol. Chem.* **288**, 21688–21702 (2013).
40. T. Wagner, "Structural insights into mycobacterial central carbon metabolism: The catalytic mechanisms and regulatory properties of alpha-ketoglutarate decarboxylase (KGD)," thesis, University Pierre and Marie Curie, Paris, France (2011).
41. K. Sharma, M. Gupta, M. Pathak, N. Gupta, A. Koul, S. Sarangi, R. Baweja, Y. Singh, Transcriptional control of the mycobacterial embCAB operon by PknH through a regulatory protein, EmbR, *in vivo*. *J. Bacteriol.* **188**, 2936–2944 (2006).
42. K. J. Kieser, E. J. Rubin, How sisters grow apart: Mycobacterial growth and division. *Nat. Rev. Microbiol.* **12**, 550–562 (2014).
43. P. D. Mace, Y. Wallez, M. F. Egger, M. K. Dobaczewska, H. Robinson, E. B. Pasquale, S. J. Riedl, Structure of ERK2 bound to PEA-15 reveals a mechanism for rapid release of activated MAPK. *Nat. Commun.* **4**, 1681 (2013).
44. J. Oberoi, D. M. Dunn, M. R. Woodford, L. Mariotti, J. Schulman, D. Bourboulia, M. Mollapour, C. K. Vaughan, Structural and functional basis of protein phosphatase 5 substrate specificity. *Proc. Natl. Acad. Sci. U.S.A.* **113**, 9009–9014 (2016).
45. K. Matsuzaki, A. Shinohara, M. Shinohara, Forkhead-associated domain of yeast Xrs2, a homolog of human Nbs1, promotes nonhomologous end joining through interaction with a ligase IV partner Protein, Lif1, Lif1. *Genetics* **179**, 213–225 (2008).
46. Z. Cai, N. H. Chehab, N. P. Pavletich, Structure and activation mechanism of the CHK2 DNA damage checkpoint kinase. *Mol. Cell* **35**, 818–829 (2009).
47. Y.-S. Huoh, K. M. Ferguson, The pellino E3 ubiquitin ligases recognize specific phosphothreonine motifs and have distinct substrate specificities. *Biochemistry* **53**, 4946–4955 (2014).
48. N. Dephoure, K. L. Gould, S. P. Gygi, D. R. Kellogg, Mapping and analysis of phosphorylation sites: A quick guide for cell biologists. *Mol. Biol. Cell* **24**, 535–542 (2013).
49. C. Narayanan, D. Bernard, N. Doucet, Role of conformational motions in enzyme function: Selected methodologies and case studies. *Catalysts* **6**, 81 (2016).
50. R. J. Swett, G. A. Cisneros, A. L. Feig, Disruption of intrinsic motions as a mechanism for enzyme inhibition. *Biophys. J.* **105**, 494–501 (2013).
51. C. A. Dodson, T. Haq, S. Yeoh, A. M. Fry, R. Bayliss, The structural mechanisms that underpin mitotic kinase activation. *Biochem. Soc. Trans.* **41**, 1037–1041 (2013).
52. L. R. Pearce, D. Komander, D. R. Alessi, The nuts and bolts of AGC protein kinases. *Nat. Rev. Mol. Cell Biol.* **11**, 9–22 (2010).
53. B. Boitel, M. Ortiz-Lombardia, R. Durán, F. Pompeo, S. T. Cole, C. Cerveñansky, P. M. Alzari, PknB kinase activity is regulated by phosphorylation in two Thr residues and dephosphorylation by PstP, the cognate phospho-Ser/Thr phosphatase, in *Mycobacterium tuberculosis*. *Mol. Microbiol.* **49**, 1493–1508 (2003).
54. E. Frachon, V. Bondet, H. Munier-Lehmann, J. Bellalou, Multiple microfermentor battery: A versatile tool for use with automated parallel cultures of microorganisms producing recombinant proteins and for optimization of cultivation protocols. *Appl. Environ. Microbiol.* **72**, 5225–5231 (2006).
55. S. van den Berg, P.-Å. Löfdahl, T. Härd, H. Berglund, Improved solubility of TEV protease by directed evolution. *J. Biotechnol.* **121**, 291–298 (2006).
56. P. Schuck, Size-distribution analysis of macromolecules by sedimentation velocity ultracentrifugation and Lamm equation modeling. *Biophys. J.* **78**, 1606–1619 (2000).
57. A. Ortega, D. Amorós, J. García de la Torre, Prediction of hydrodynamic and other solution properties of rigid proteins from atomic- and residue-level models. *Biophys. J.* **101**, 892–898 (2011).
58. W. Kabsch, XDS. *Acta Crystallogr. D Biol. Crystallogr.* **66**, 125–132 (2010).
59. P. R. Evans, G. N. Murshudov, How good are my data and what is the resolution? *Acta Crystallogr. D Biol. Crystallogr.* **69**, 1204–1214 (2013).
60. A. J. McCoy, R. W. Grosse-Kunstleve, P. D. Adams, M. D. Winn, L. C. Storoni, R. J. Read, *Phaser* crystallographic software. *J. Appl. Cryst.* **40**, 658–674 (2007).
61. P. Emsley, K. Cowtan, *Coot*: Model-building tools for molecular graphics. *Acta Crystallogr. D Biol. Crystallogr.* **60**, 2126–2132 (2004).
62. G. Bricogne, E. Blanc, M. Brandl, C. Flensburg, P. Keller, P. Paciorek, P. Roversi, A. Sharff, O. Smart, C. Vonrhein, T. Womack. BUSTER version 2.10.3. Cambridge, United Kingdom: Global Phasing Ltd. (2017).
63. K.-A. Boulahya, E. Guedon, S. Delaunay, C. Schultz, J. Boudrant, M. Bott, J.-L. Goergen, OdhI dephosphorylation kinetics during different glutamate production processes involving *Corynebacterium glutamicum*. *Appl. Microbiol. Biotechnol.* **87**, 1867–1874 (2010).
64. S. Pennell, S. Westcott, M. Ortiz-Lombardía, D. Patel, J. Li, T. J. Nott, D. Mohammed, R. S. Buxton, M. B. Yaffe, C. Verma, S. J. Smerdon, Structural and functional analysis of phosphothreonine-dependent FHA domain interactions. *Structure* **18**, 1587–1595 (2010).
65. L. J. Alderwick, V. Molle, L. Kremer, A. J. Cozzone, T. R. Dafforn, G. S. Besra, K. Fütterer, Molecular structure of EmbR, a response element of Ser/Thr kinase signaling in *Mycobacterium tuberculosis*. *Proc. Natl. Acad. Sci. U.S.A.* **103**, 2558–2563 (2006).

Acknowledgments: We thank R. Biondi for assistance with kinase assays and helpful discussions, A. Haouz and P. Weber (Crystallography Platform, C2RT, Institut Pasteur) for help with robot-driven crystallization screenings, J. Bellalou (Recombinant Proteins Platform, C2RT, Institut Pasteur) for help in protein production, and F. Schaeffer (Structural Microbiology Unit, Institut Pasteur) for assistance with ITC measurements. We acknowledge the synchrotron sources Soleil (Saint-Aubin, France) and ESRF (Grenoble, France) for granting access to their facilities and their staff members for helpful assistance. **Funding:** This work was partially supported by grants from the Institut Pasteur, the CNRS, and the European Commission's Seventh Framework Programme (MM4TB, grant no. 260872). M.N.L. received postdoctoral fellowships from EMBO (European Molecular Biology Organization) and FRM (Fondation pour la Recherche Medicale, France). **Author contributions:** H.M.O., M.B., and P.M.A. designed the experiments; T.W., G.A.-L., V.H., M.-N.L., H.M.O., N.B., and B.V.-L.N. performed the experiments; T.W., G.A.-L., M.-N.L., S.H., B.R., H.M.O., M.B., and P.M.A. analyzed the data; T.W., G.A.-L., M.-N.L., H.M.O., M.B., and P.M.A. wrote the manuscript. **Competing interests:** The authors declare that they have no competing interests. **Data and materials availability:** The atomic coordinates and structure factors of the four crystal structures were deposited in the PDB with codes 6I2P (*Mt*PknB$_{CD,L33A}$-*Mt*GarA), 6I2Q (*Ms*KGD$_{\Delta360}$-*Ms*GarA$_{\Delta44}$), 6I2R (*Ms*KGD$_{\Delta360,R802A}$-*Ms*GarA$_{\Delta44}$), and 6I2S (*Ms*KGD$_{\Delta360,R802A}$-*Ms*GarA$_{\Delta44}$, 2-oxoglutarate soak). All other data needed to evaluate the conclusions in the paper are present in the paper or the Supplementary Materials.

Submitted 15 November 2018
Accepted 18 April 2019
Published 7 May 2019
10.1126/scisignal.aav9504

Citation: T. Wagner, G. André-Leroux, V. Hindie, N. Barilone, M.-N. Lisa, S. Hoos, B. Raynal, B. Vulliez-Le Normand, H. M. O'Hare, M. Bellinzoni, P. M. Alzari, Structural insights into the functional versatility of an FHA domain protein in mycobacterial signaling. *Sci. Signal.* **12**, eaav9504 (2019).

Structural insights into the functional versatility of an FHA domain protein in mycobacterial signaling

Tristan Wagner, Gwénaëlle André-Leroux, Valérie Hindie, Nathalie Barilone, María-Natalia Lisa, Sylviane Hoos, Bertrand Raynal, Brigitte Vulliez-Le Normand, Helen M. O'Hare, Marco Bellinzoni and Pedro M. Alzari

Sci. Signal. **12** (580), eaav9504.
DOI: 10.1126/scisignal.aav9504

An FHA domain with dual specificity

Forkhead-associated (FHA) domains participate in phosphorylation-dependent signaling pathways by binding to phosphothreonine. As part of a signaling pathway that controls glutamate metabolism, the mycobacterial FHA domain–containing protein GarA binds to both phosphorylated upstream partners, such as the kinases PknB and PknG, and nonphosphorylated downstream partners, such as the 2-oxoglutarate decarboxylase KGD. Through biochemical and structural studies, Wagner *et al.* found that the interactions of GarA with both phosphorylated PknB and nonphosphorylated KGD were mediated by the phosphate-binding pocket of the FHA domain, which bound to a phosphothreonine in the activation loop of PknB and to a phosphomimetic aspartate residue in KGD. In addition to illustrating the dual binding specificity of GarA, these findings demonstrate a physiological role for aspartate as a phosphomimetic.